A compatible method to summarise the Low- and High-Cycle fatigue test results of ductile irons and structural steels

B. Atzori, G. Meneghetti. M. Ricotta
Dipartimento di Ingegneria Industriale, Università di Padova, via Venezia 1, 35131, Padova

S. Masaggia
Zanardi Fonderie Spa, via Nazionale 3, 37046 Minerbe, Verona

ABSTRACT. In this paper the low and high cycle fatigue behaviour of ten structural materials is analysed in terms of strain-life, stress-life and cyclic stress-strain curves. Push-pull, strain-controlled fatigue tests are performed and then the experimental data are processed according to the Standards in force as well as following a recent procedure proposed by the authors which ensures the compatibility conditions are satisfied. As a result, a three dimensional representation of the experimental data in a stress-strain-life diagram can be drawn. The stress-life, strain-life and cyclic stress-strain curves are the projection of a unique three-dimensional curve onto the co-ordinate planes.

KEYWORDS. Low cycle fatigue; High cycle fatigue; Ductile iron; Manson-Coffin curve; S-N curve; Cyclic stress-strain curve; Compatibility conditions; Austempered ductile iron.

INTRODUCTION

The strain-based approach finds applications in fatigue life estimation when yielding is involved and proves to be a useful method for estimating the fatigue life of structural and mechanical components mainly in the Low Cycle Fatigue (LCF) region. The relation between the total strain amplitude ea and the number of reversals to failure $2N_f$ is usually determined by means of completely reversed, strain-controlled, constant amplitude fatigue tests. The results are interpolated by means of the Manson-Coffin equation [1], in which the total applied strain amplitude ε_a is divided in its elastic ($\varepsilon_{a,el}$) and plastic ($\varepsilon_{a,pl}$) components:

$$\varepsilon_a = \varepsilon_{a,el} + \varepsilon_{a,pl} = \frac{\sigma_f'}{E}\left(2N_f\right)^b + \varepsilon_f'\left(2N_f\right)^c \quad (1)$$

where σ_f' is the fatigue strength coefficient, E the modulus of elasticity, b the fatigue strength exponent, ε_f' the fatigue ductility coefficient, c the fatigue ductility exponent and $2N_f$ the number of reversals to failure. Besides the modulus of elasticity E, Eq. 1 contains four unknown material parameters σ_f', b, ε_f' and c that are evaluated by fitting the experimental fatigue data.
Conversely, in the case of High Cycle Fatigue (HCF) region, the stress-based approach is usually adopted. In this case, the stress-life law is described in terms of reversals to failure in the following form:

$$\sigma_a^k \cdot 2N_f = \sigma_A^k \cdot 2N_A \quad (2)$$

where σ_a is the applied stress amplitude, k the inverse slope of fatigue curve, σ_A the reference fatigue strength evaluated at N_A number of cycles to failure (e.g. 2 million cycles). The unknown parameters of Eq. 2 (k, σ_A) are evaluated by fitting the experimental fatigue data.

Usually Eq. 2 and the expressions of the elastic and the plastic components of Eq. 1 are linearised by introducing log-log scales and then the unknown parameters can be calculated following the recommendations reported in proper Standards [2]. This practice consists in a statistical analysis of linear or linearised fatigue data, in which the controlled variable (namely, stress or strain) is considered as independent and the number of cycles to failure as a dependent variable. It is assumed that the number of cycles to failure is log-normally distributed and that the variance of log-life is constant over the entire range of the independent variable used in testing.
The stabilised stress-strain relationship due to cycling loadings is usually described by means of the following equation:

$$\varepsilon = \varepsilon_{el} + \varepsilon_{pl} = \frac{\sigma}{E} + \left(\frac{\sigma}{K'}\right)^{\frac{1}{n'}} \tag{3}$$

where K' and n' are the hardening coefficients relevant to the stabilised cyclic curve. The material parameters K' and n' are usually evaluated by fitting the experimental data obtained from the same strain-controlled fatigue tests adopted to determine the parameters of Eq. 1.
By equating elastic and plastic components of the strain amplitude derived from Eq. 1 and Eq. 3, respectively, and eliminating the dependence on the number of cycles to failure, the so-called compatibility equations can be obtained [1]:

$$n' = \frac{b}{c} \qquad K' = \frac{\sigma_f'}{\left(\varepsilon_f'\right)^{b/c}} \tag{4}$$

Eq. 4 shows that only five among the seven material parameters appearing in Eq. 1 and Eq. 3 are independent.
Recently, the problem of a unified treatment of the stress-strain-life relationships has been dealt with leading to a three dimensional representation of the experimental results [3,4], which is reported in Fig. 1. The advantage of such a unique representation is that the material parameters involved in Eq. 1-3 satisfy the compatibility conditions. Following classical and widely adopted approaches, Eq. 1 and 2 are derived by fitting results of strain-controlled or stress-controlled fatigue tests, respectively, according to ref. [2]. However, when dealing with strain-controlled tests, it is common practise to derive strain-life (Eq. 1) and cyclic stress-strain (Eq. 3) curves by treating the data as separate sets one from another, even if they belong to a unique series of experiments. This implies that the compatibility conditions are satisfied only approximately [1].
In this paper, the novel procedure for fatigue data analysis that satisfies the compatibility conditions is first summarised. Then the fatigue behaviour of ten structural materials including ferritic, pearlitic, isothermed and austempered ductile irons and one structural steel are analysed and compared.

THEORETICAL BACKGROUND

The theoretical model for the analysis of strain-controlled fatigue test results has been recently presented [4] and it is based on the idea proposed by Nieslony et al. [3] of representing the fatigue data in a strain-stress-life space. Its starting point is the evaluation of the stress-life curve (Eq. 2) as well as of the plastic strain-life curve (second contribution of Eq. 1) according to ref. [2]. In this paper the procedure of best fitting of a set of data according to ref. [2] will be referred to as "ASTM procedure". As a result, σ_A and k, appearing in Eq. 2, and c and ε'_f, appearing in Eq. 1, are determined by fitting the relevant experimental data.
Let us now define:

$$x = \log\left(\varepsilon_{a,pl}\right) \qquad y = \log\left(\sigma_a\right) \qquad z = \log\left(2N_f\right) \tag{5}$$

So that the plastic component of Eq. 1 and the Eq. 2 can be linearised.
A straight line in a three-dimensional space can be defined as intersection of the so-called "plastic" and "S-N" planes in Fig. 1:

$$\begin{cases} ky + z - \left[k\log\sigma_A + \log\left(2N_A\right)\right] = 0 \\ x - cz - \log\left(\varepsilon_f'\right) = 0 \end{cases} \tag{6}$$

where the first equation represents a plane parallel to x-axis (S-N plane) and the second a plane parallel to the y-axis (plastic plane).

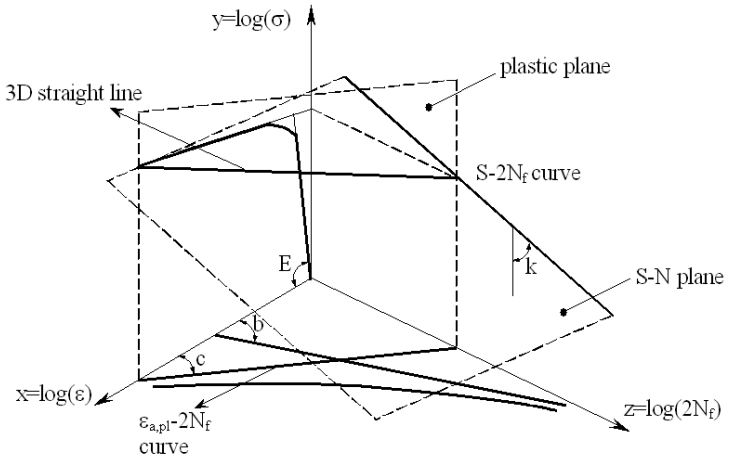

Figure 1: Schematic view of proposed methodology.

By projecting Eq. 6 to y-x (σ-ε) plane, the plastic contribution of Eq. 3 is obtained graphically. Then the hardening parameters can be evaluated as follows:

$$n' = -(c \cdot k)^{-1} \qquad K' = \sigma_A \left(2N_A\right)^{\frac{1}{k}} \cdot \left(\varepsilon_f'\right)^{\frac{1}{c \cdot k}} \tag{7}$$

By considering the elastic component of Eq. 1, the stress amplitude can be written as:

$$\sigma_a = \sigma_f' \cdot \left(2N_f\right)^b \tag{8}$$

which has the same mathematical form of Eq. 2. Therefore comparison of Eq. 8 with Eq. 2 leads to:

$$b = -1/k \qquad \sigma_f' = \sigma_A \cdot \left(2N_A\right)^{1/k} \tag{9}$$

When fitting the elastic component of Eq. 1, b and σ_f' values calculated according to Eq. 9 must be used, while the dynamic elastic modulus E is the fitting parameter. Finally, by substituting Eq. 9 into Eq. 7, it can be verified that the compatibility conditions (Eq. 4) are obtained.

MATERIALS AND TEST PROCEDURES

In this paper the fatigue behaviour of nine cast irons and one structural steel is analysed by carrying out strain-controlled axial fatigue tests according to ref. [5] on specimens' geometry reported in Figure 2. A MTS FPF10 servo-hydraulic testing machine equipped with a 100 kN load cell, a Trio Sistemi RT3 digital controller and a MTS extensometer 632.12C-20 having a gauge length of 25 mm were used. The fatigue tests were carried out by imposing a sinusoidal wave form characterised by a nominal strain ratio R_ε (defined as the ratio between the minimum and the maximum strain) equal to –1. Test frequencies between 0.25 and 3 Hz were adopted.

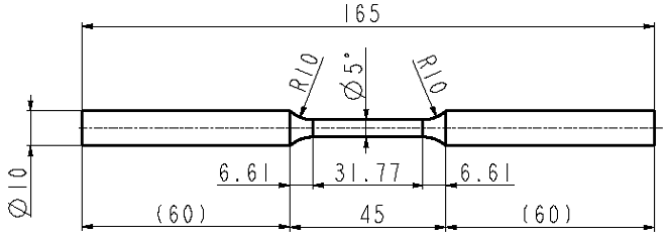

Figure 2: Adopted specimens' geometry for constant amplitude, strain-controlled fatigue tests (°: Φ 7 mm only for DI-400, dimensions in mm).

In the case of cast irons, fatigue tests were interrupted in correspondence to the complete failure of the specimen. Conversely, for the 42CrMo4 Q&T structural steel, the number of cycles to failure was defined by a 30% load decrease. During fatigue tests the hysteresis loops were measured by using the signals acquired from the load cell and the extensometer. Stabilized hysteresis loops were considered at half the fatigue life of specimens, while long-run tests up to $5 \cdot 10^6$ cycles in the elastic regime have been carried out by switching to stress controlled mode and using test frequency of 20 Hz [5].

Material	Microstructure	Nod/ mm²	E_s [GPa]	σ_R [MPa]	σ_{p02} [MPa]	A [%]	HB	C	Si	Mn	Cu
DI-400 °	Ferritic	220	160	440	305	19	150	3.30	2.80	0.10	0.07
DI-600 °	Ferritic-pearlitic	310	165	722	426	10	220	3.70	2.20	0.18	0.44
DI-700 °	Pearlitic-ferritic	244	161	805	487	8	244	3.80	2.40	0.20	1.10
IDI PD 06 °°	Pearlitic-ferritic (interconnected)	280	170	855	592	8	260	3.50	2.20	0.10	0.10
IDI °°	Pearlitic-ferritic (interconnected)	220	170	758	455	10	240	3.70	2.40	0.10	0.07
ADI 800*	Ausferritic	244	170	858	551	15	270	3.80	2.61	0.10	0.83
ADI 1050 (1st series) *	Ausferritic	244	163	1110	794	13	330	3.83	2.41	0.10	0.93
ADI 1050 (2nd series) *	Ausferritic	244	161	1160	831	12	350	3.50	2.80	0.10	0.93
ADI 1200 *	Ausferritic	244	148	1330	1046	7	370	3.40	2.91	0.10	1.10
42CrMo4 Q&T **	Sorbitic	-	210	1026	882	14	305	0.38	0.15	0.10	0.02

°: according to UNI EN 1563 °°: according to ZANARDI STD 101: 2007
*: according to ISO 17804 **: according to UNI EN 10083-1

Table 1: Static mechanical properties, Brinell hardness and composition of tested materials

The static properties of tested materials were measured by using a DARTEK M1000/RF servo-hydraulic testing machine equipped with a load cell of 300 kN, Zwick/Roell BZC-MHDA.03-A-2 digital controller and Zwick extensometer. At least three static tests for each material have been carried out by imposing an initial crossheads separation rate equivalent to a stress rate of 27 MPa·s-1 until σ_{p02}; then the crossheads separation rate was increased to obtain 0.008 s-1 until the specimen's failure. The mean value of static elastic modulus E_s, engineering proof stress σ_{p02}, engineering tensile strength σ_R and percentage deformation after fracture A% are summarised in Tab. 1, where the results of Brinell hardness tests and the chemical composition are also reported.

FATIGUE TEST RESULTS

Figs. 3-7 report the recorded stress amplitude σ_a versus the number of reversals. In particular, Figs. 3-5(a) show that σ_a increases, thus denoting the hardening behaviour of DI-400, DI-600, DI-700, IDI PD 06 and IDI and does not attain a stabilised value. In the case of ADI 800 (see Fig. 5(b)), ADI 1050 1st series, ADI 1050 2nd series (see Fig. 6) as well as for ADI 1200 (see Fig. 7(a)) the recorded stress amplitude slightly decreases, if the applied strain level is greater than 0.5%, and does not reach a stabilised value. However, by comparing the monotonic with the cyclic stress-strain curves (see Figs. 20(b)-22(a)), it is seen that the ADI ductile irons are characterised by a hardening behaviour, which indicates that initially the material strain hardens, but later on during the test a slight softening occurs. If the applied strain amplitude is lower than 0.5%, nearly elastic strains are applied, so that the material response is stable during the fatigue test. In the case of 42CrMo4 Q&T structural steel, Fig. 7(b) shows that the recorded stress amplitude decreases during the fatigue test indicating the softening behaviour of this material. Accordingly, Fig. 22(b) shows that the cyclic stress-strain curve is below the monotonic one. Such a behaviour is in agreement with the data available in the literature [7].

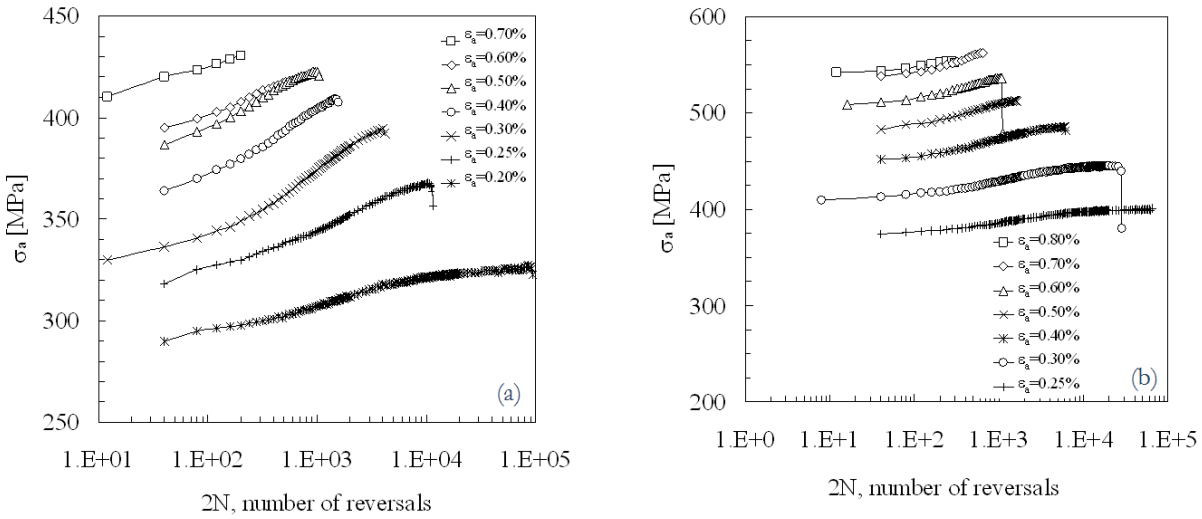

Figure 3: Stress amplitude versus number of reversals for (a) DI-400 and (b) DI-600.

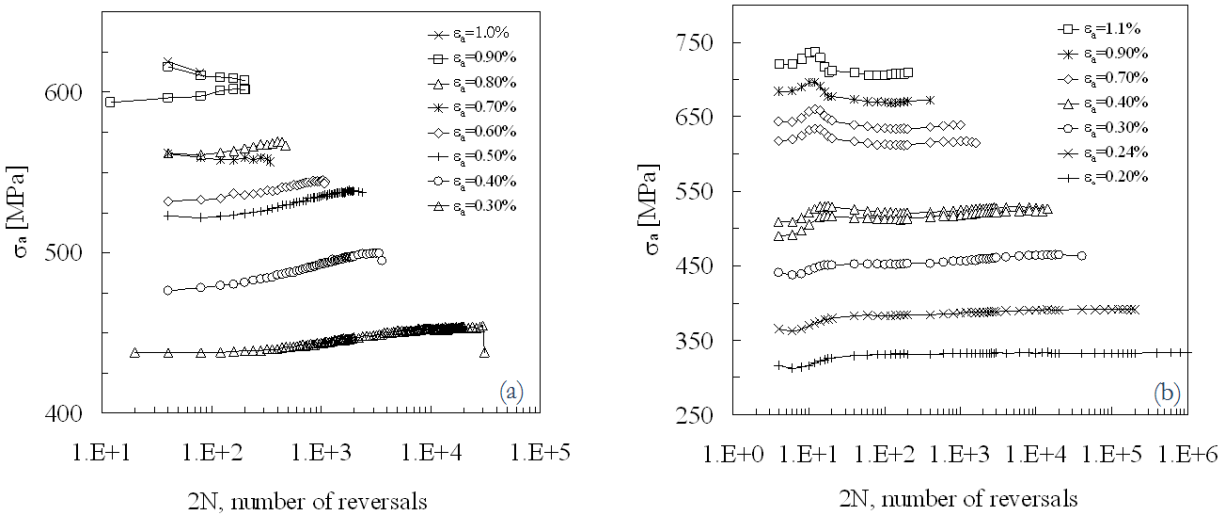

Figure 4: Stress amplitude versus number of reversals for (a) DI-700 and (b) IDI PD 06.

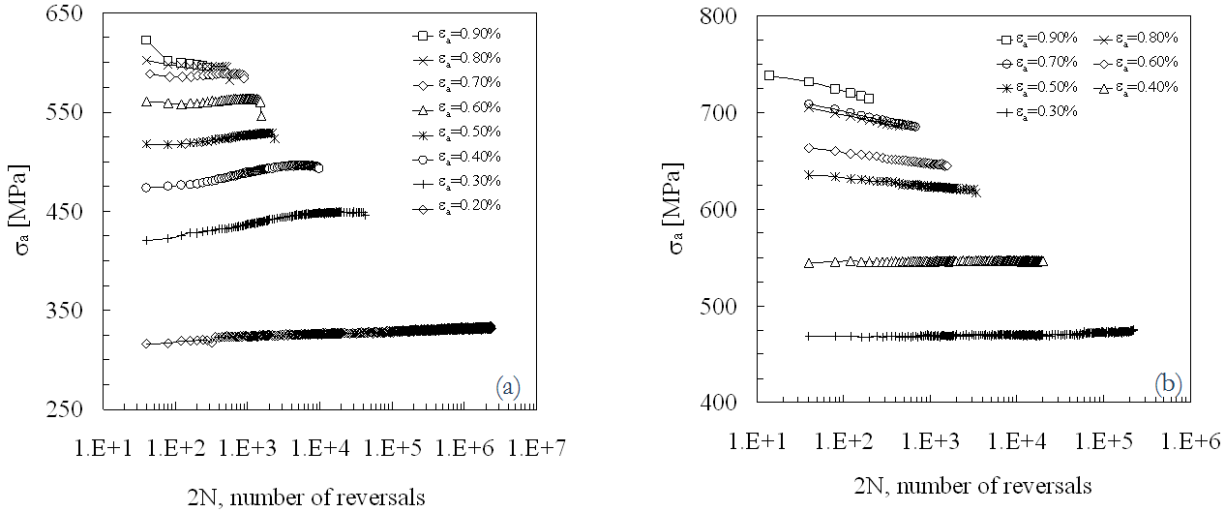

Figure 5: Stress amplitude versus number of reversals for (a) IDI and (b) ADI 800

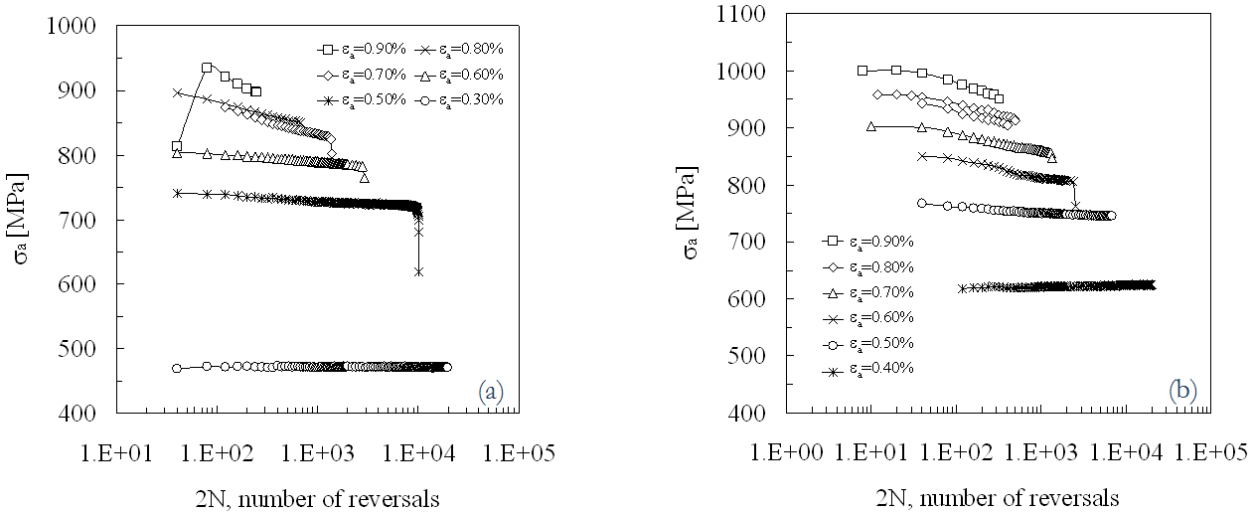

Figure 6: Stress amplitude versus number of reversals for (a) ADI 1050 (1st series) and (b) ADI 1050' (2nd series).

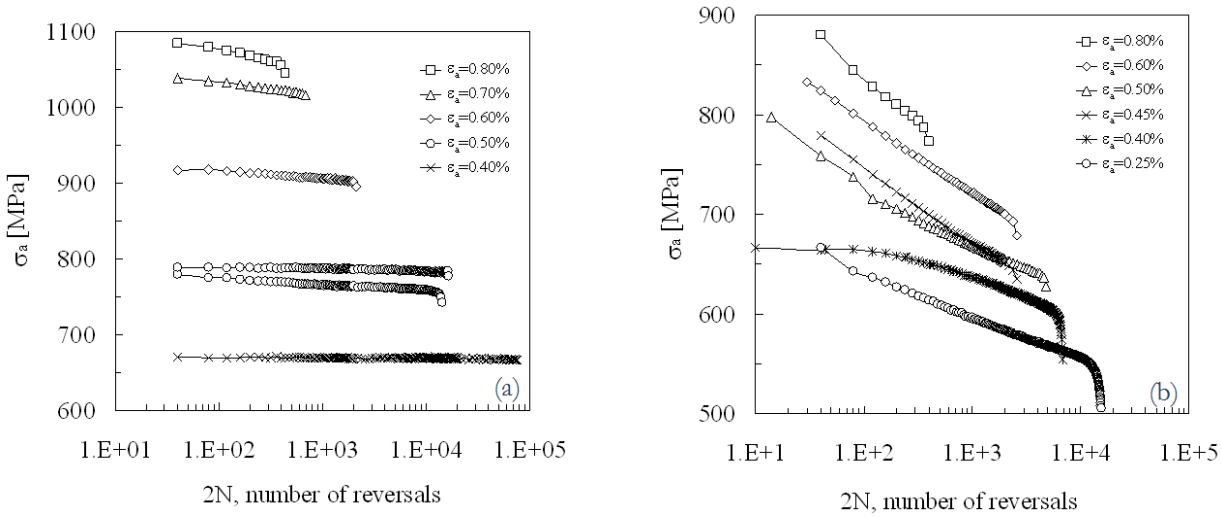

Figure 7: Stress amplitude versus number of reversals for (a) ADI 1200 and (b) 42CrMo4 Q&T.

STRAIN LIFE CURVES

Due to the observed cyclic behaviour of tested materials, the strain-life curves were evaluated according to ASTM Standard [2] as well as to the proposed methodology, by considering in both cases the $\varepsilon_{a,el}$ and $\varepsilon_{a,pl}$ values recorded at 50% of the total fatigue life. Moreover, the plastic contribution in Eq. 1 was calculated by fitting only the experimental data with plastic strains greater than a limit value ε_0, according to Williams [6] and Nieslony [3]. On the basis of the accuracy of adopted experimental device, the limit value was set equal to 0.004% (40 με). Finally, the plastic component of the strain amplitude was evaluated by considering the width of the recorded hysteresis loops. Results are reported in Figs. 8-12.

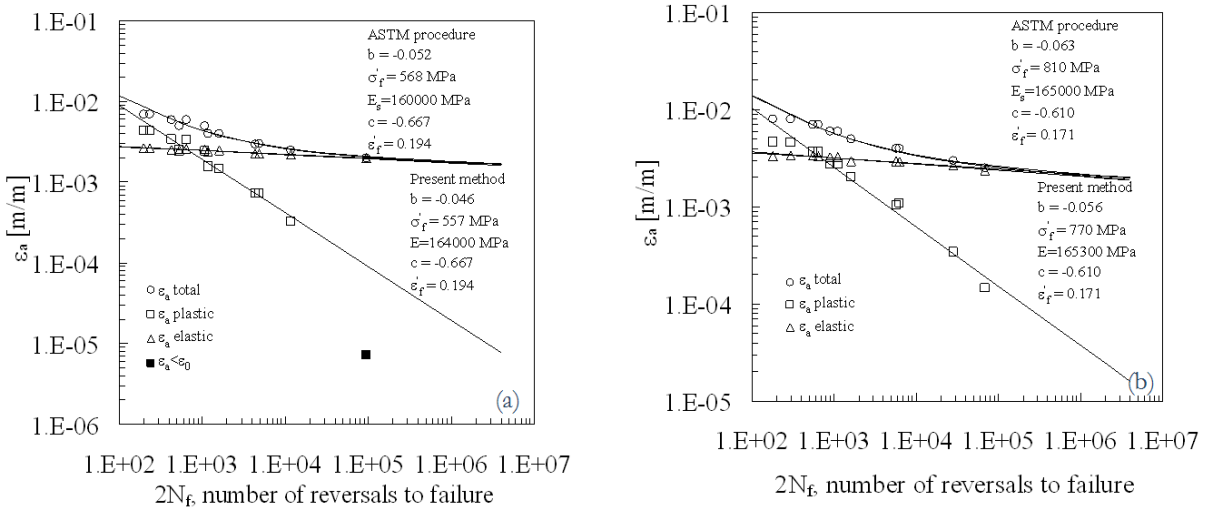

Figure 8: Manson-Coffin curves for (a) DI-400 and (b) DI-600.

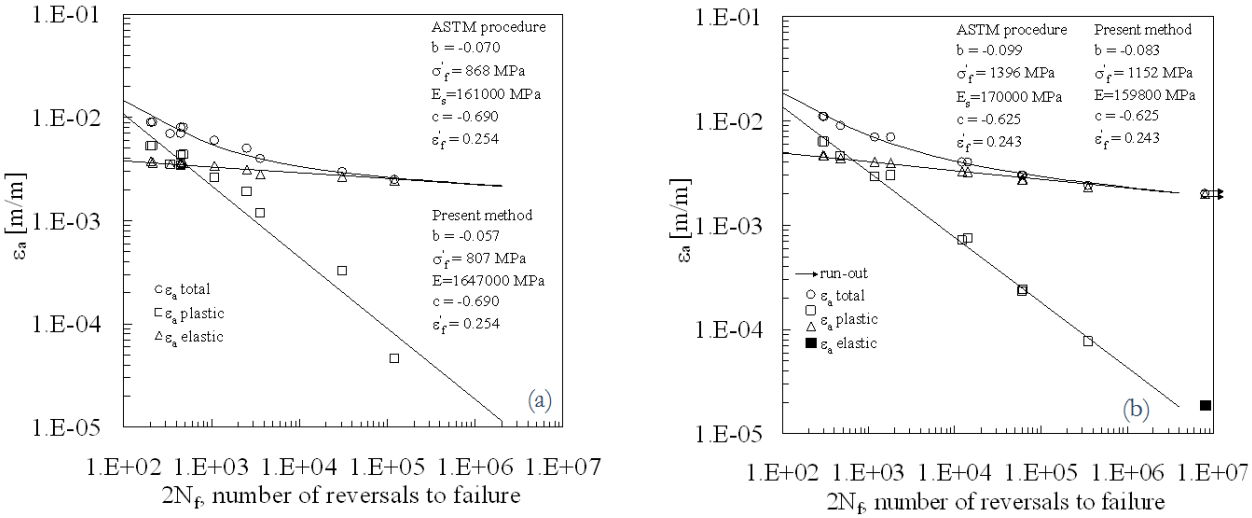

Figure 9: Manson-Coffin curves for (a) DI-700 and (b) IDI PD 06.

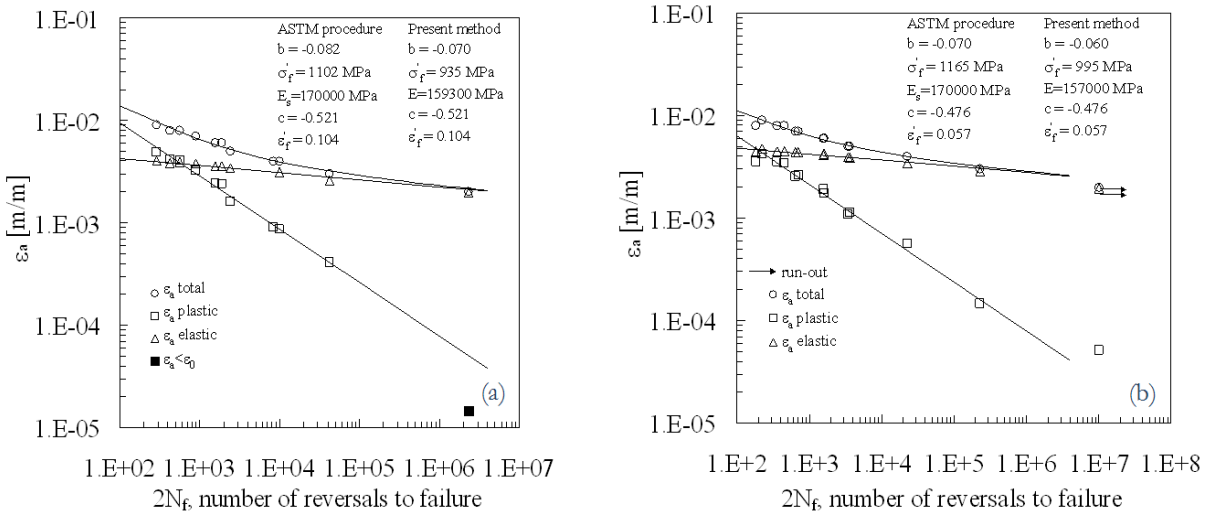

Figure 10: Manson-Coffin curves for (a) IDI and (b) ADI 800.

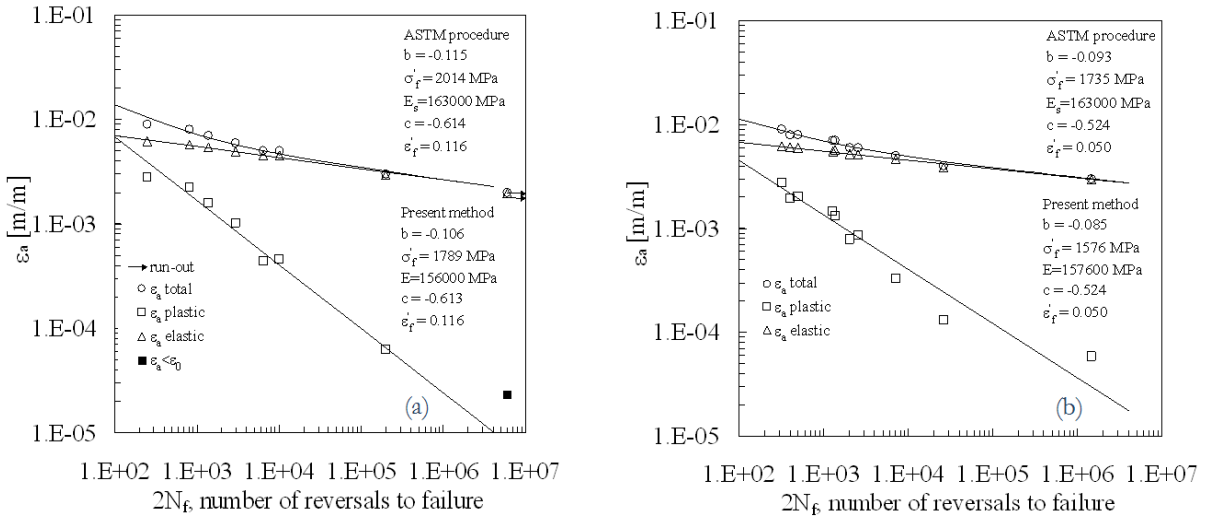

Figure 11: Manson-Coffin curves for (a) ADI 1050 (1st series) and (b) ADI 1050 (2nd series).

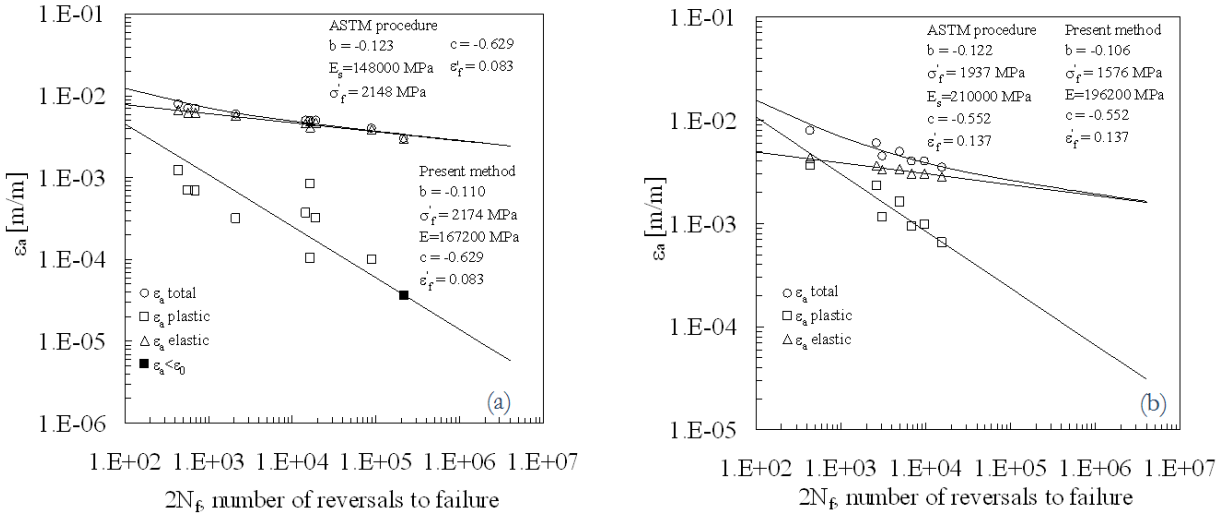

Figure 12: Manson-Coffin curves for (a) ADI 1200 and (b) 42CrMo4 Q&T.

The present method leads to results which are in accordance with the ASTM procedure; for this reason Figs. 8-12 report only the strain-life curves obtained following the present method. Nevertheless, in the same figures the material parameters evaluated following both procedures are reported.

STRESS-LIFE CURVES

Concerning stress life curves, it is worth noting that the present method is based on the initial estimation of the S-N plane, evaluated according to ref. [2], so that the "ASTM" procedure and the present method do coincide. Figs. 13-17 show the stress-life curves of tested materials in terms of stress amplitude vs. the number of reversals to failure. The inverse slope k and the fatigue strength σ_A evaluated at $N_A = 2 \cdot 10^6$ number of cycles to failure for 50% survival probability are also reported.

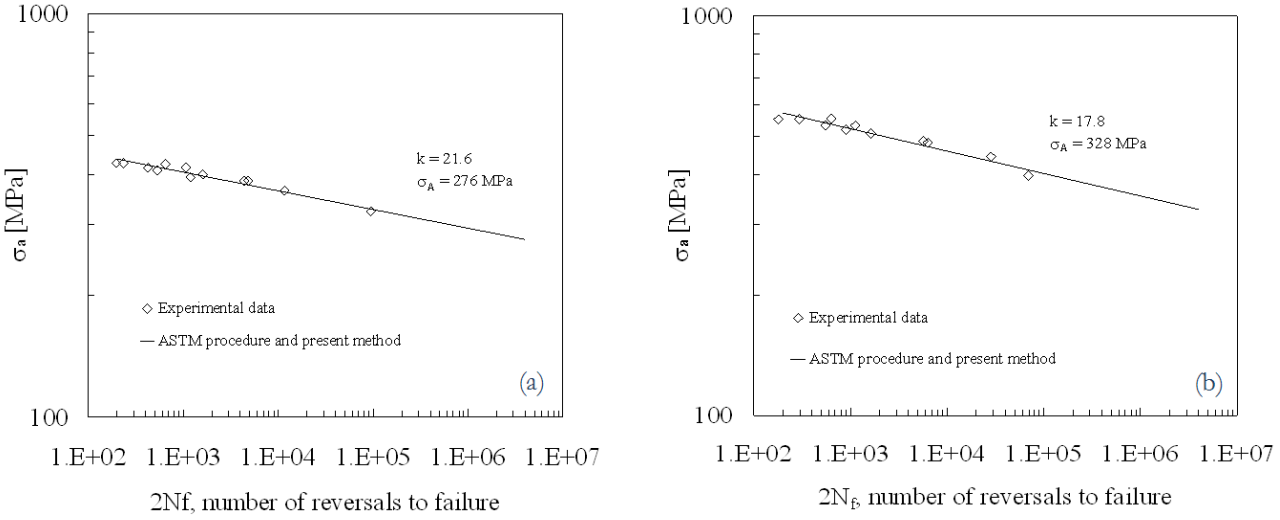

Figure 13: Stress-life curves for (a) DI-400 and (b) DI-600.

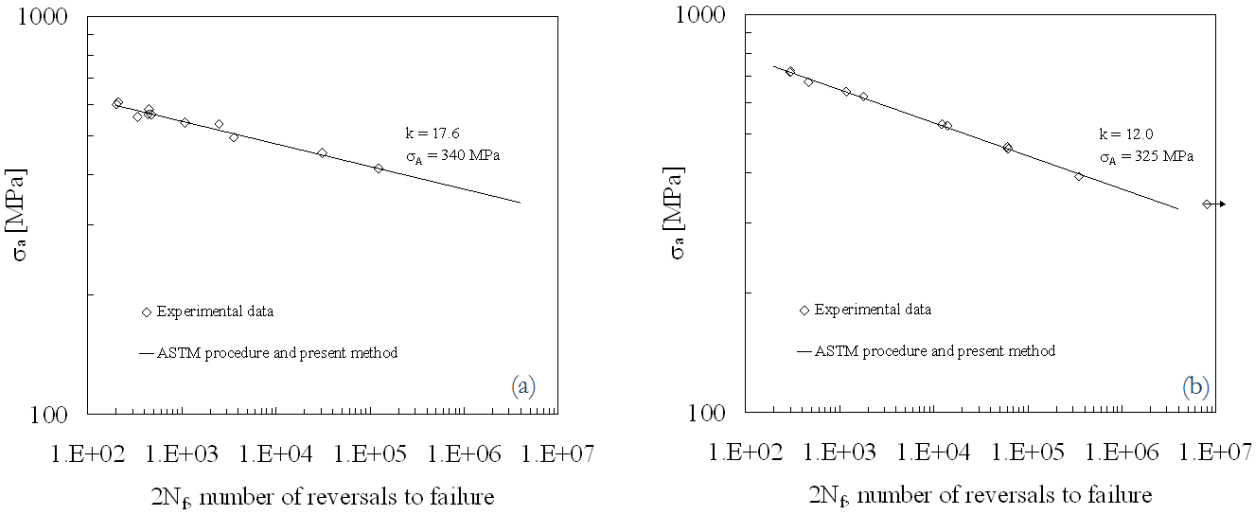

Figure 14: Stress-life curves for (a) DI-700 and (b) IDI PD 06.

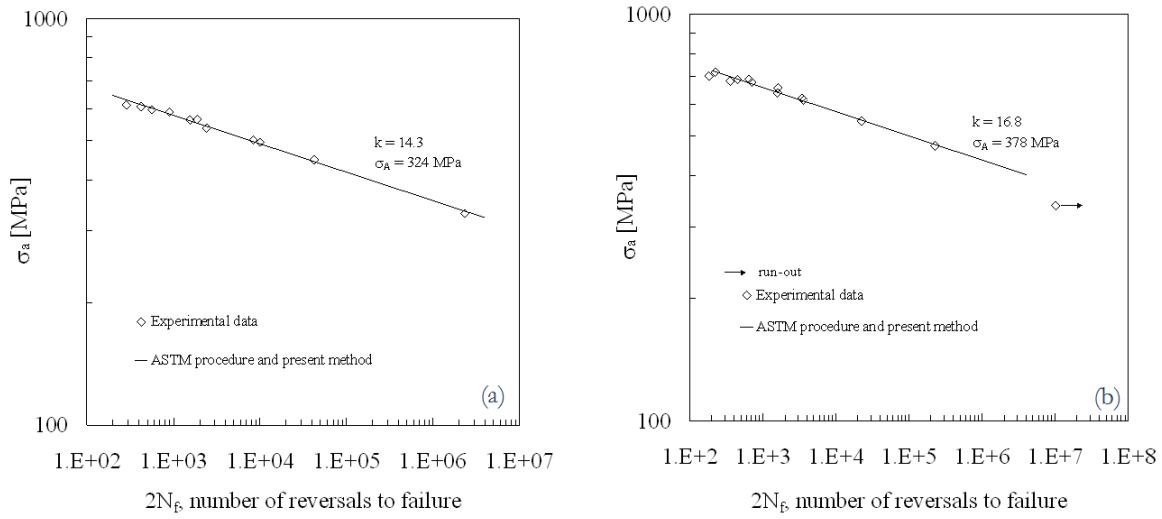

Figure 15: Stress-life curves for (a) IDI and (b) ADI 800.

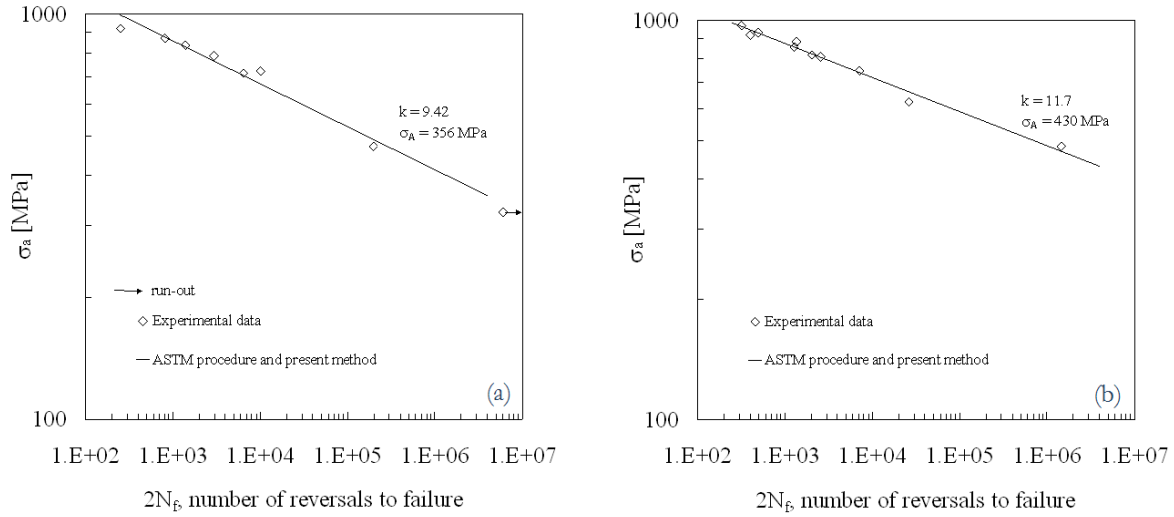

Figure 16: Stress-life curves for (a) ADI 1050 (1st series) and (b) ADI 1050 (2nd series)

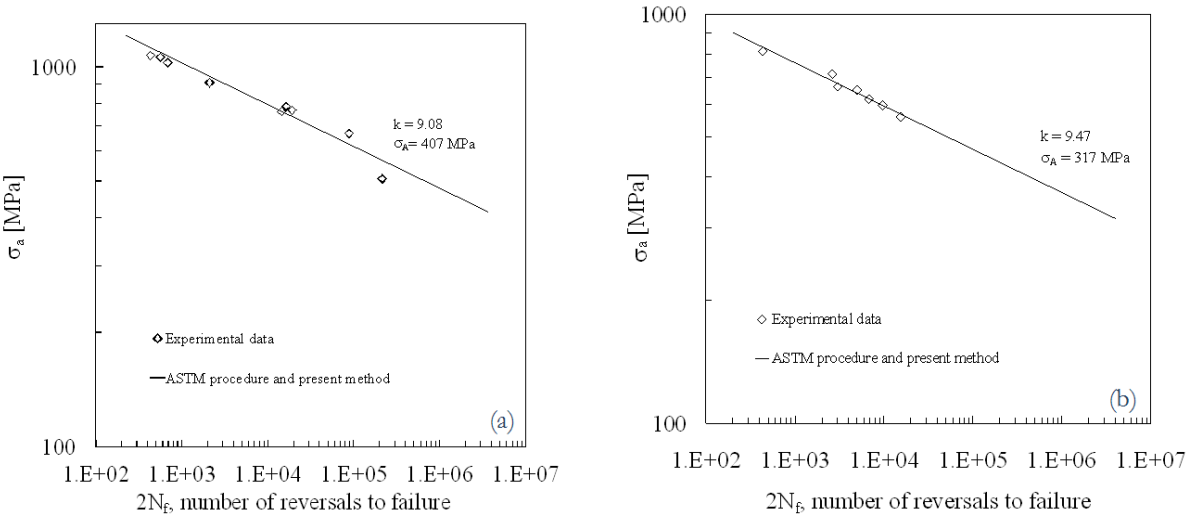

Figure 17: Stress-life curves for (a) ADI 1200 and (b) 42CrMo4 Q&T.

CYCLIC STRESS-STRAIN CURVES

As aforementioned, K' and n' are usually calculated by best fitting the experimental data, independently from the strain-life interpolations. In the present paragraph, the cyclic stress-strain curves calculated by using the best fitting method and the present procedure, which ensures compatibility in a strict sense, are presented in Figs. 18-22. Concerning the best fitting method, the Genfit least square algorithm as implemented in Mathcad® software was adopted. The stress-strain curves obtained following both procedures are plotted in Figs. 19(a), 20-22(a) and the relevant material parameters are reported too. Conversely, in the case of DI-400, DI-600, IDI PD 06 and 42CrMo4 Q&T (Figs. 18, 19(b) and 22(b), respectively) since very similar results were found between the two approaches, only the cyclic curves calculated according to the present approach are drawn. However, the hardening coefficients determined by using both methods are reported in the figures. It is worth noting that although the strain-controlled fatigue tests were carried out by imposing a nominal strain ratio Re equal to –1, the hysteresis loops recorder at 50% of fatigue life were found to be characterised by a stress ratio R_σ (defined as the ratio between the minimum and the maximum measured stress) slightly different from –1. In particular, it ranged from -1.1 to -0.98 in most cases, being -1.4 only during the high-cycle tests of the ADI 1200 material.

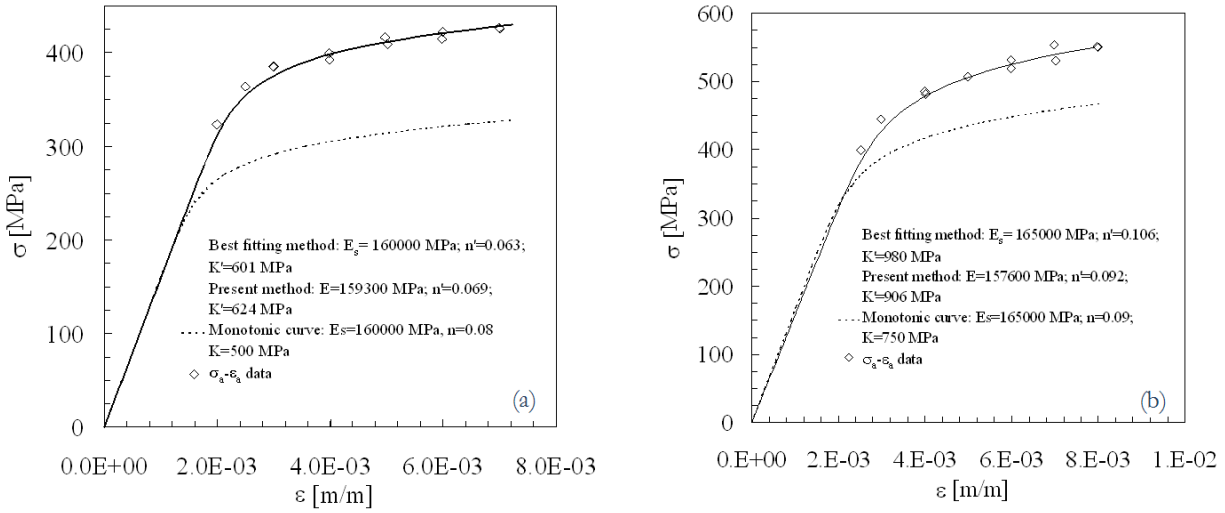

Figure 18: Cyclic stress-strain curves for (a) DI-400 and (b) DI-600.

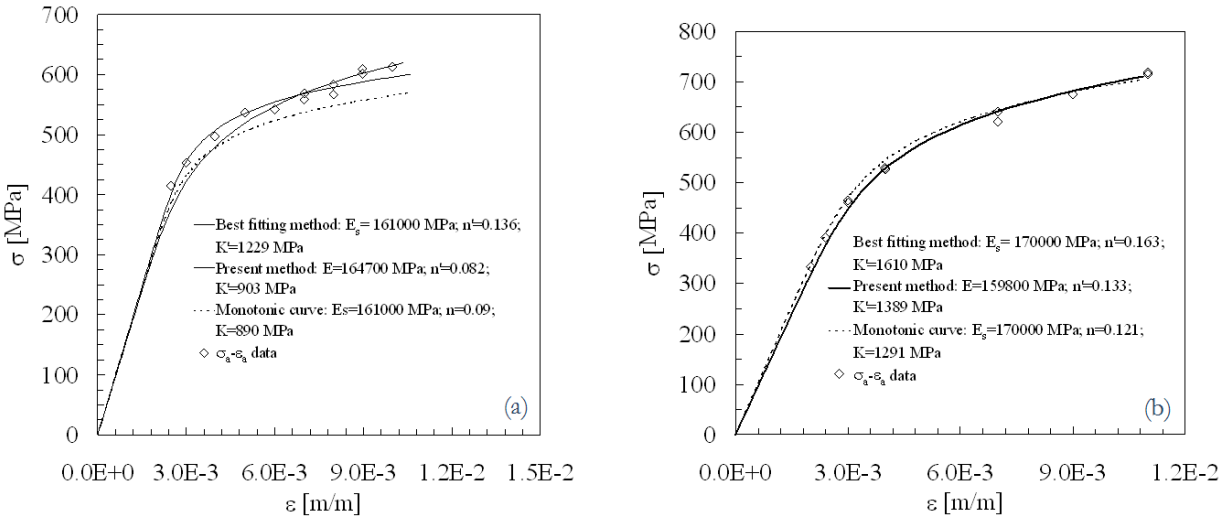

Figure 19: Cyclic stress-strain curves for (a) DI-700 and (b) IDI PD 06.

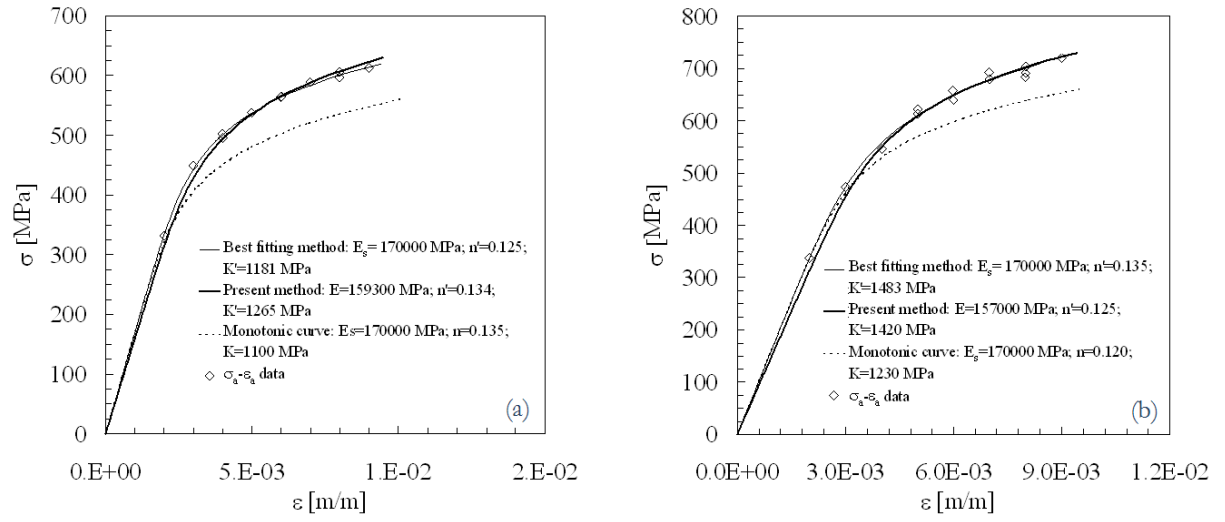

Figure 20: Cyclic stress-strain curves for (a) IDI and (b) ADI 800.

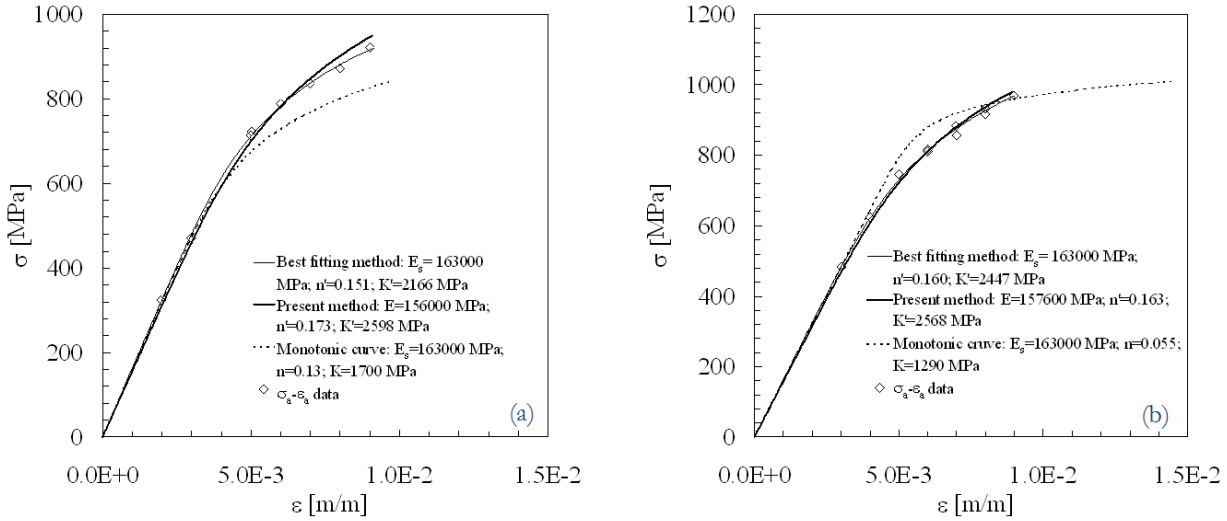

Figure 21: Cyclic stress-strain curves for (a) ADI 1050 (1st series) and (b) ADI 1050 (2nd series).

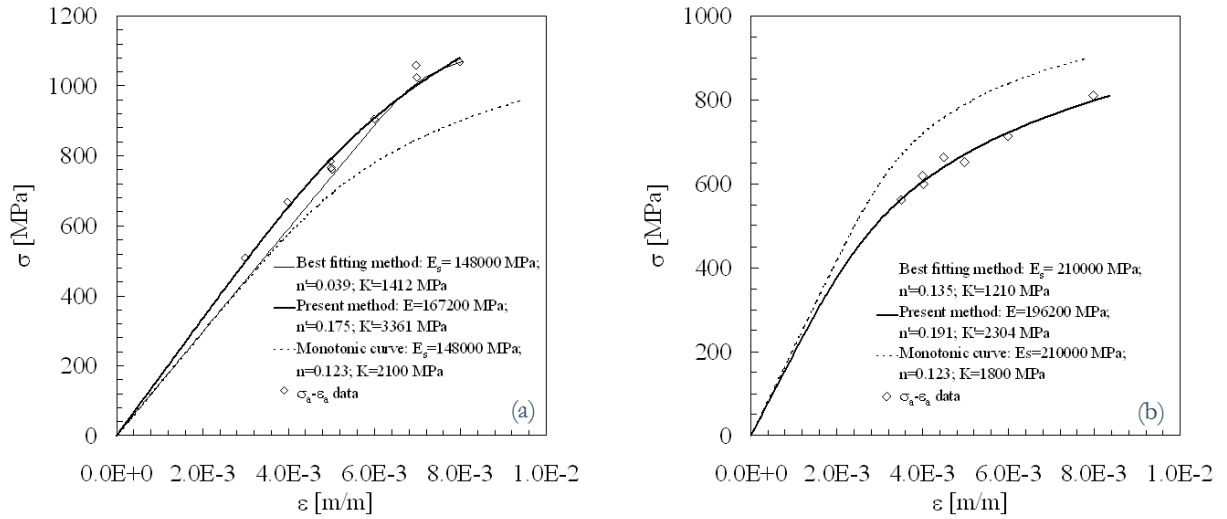

Figure 22: Cyclic stress-strain curves for (a) ADI 1200 and (b) 42CrMo4 Q&T.

DISCUSSION

In order to compare the fatigue behaviour of all tested materials, the strain-life, stress-life and stress-strain curves, evaluated according to the present procedure, are collected all together in Figs. 23(a), 23(b) and 24, respectively. Fig. 23(a) enables one to appreciate the effect of chemical composition and different microstructures on fatigue performances. As an example, IDI microstructure has been optimised for best strain-controlled low-cycle fatigue behaviour, while ADI 1050 materials show high fatigue performances in the high cycle regime.
The S-N curves and the cyclic curves shown in Fig. 23(b) and 24 enable one to consider that, for a given strain level, stresses may be significantly different from one material to another. This implies that when elastic conditions in a component governs local yielding at some critical points, both strain-life curves and cyclic stress-strain curves should be considered for a correct fatigue life estimation.

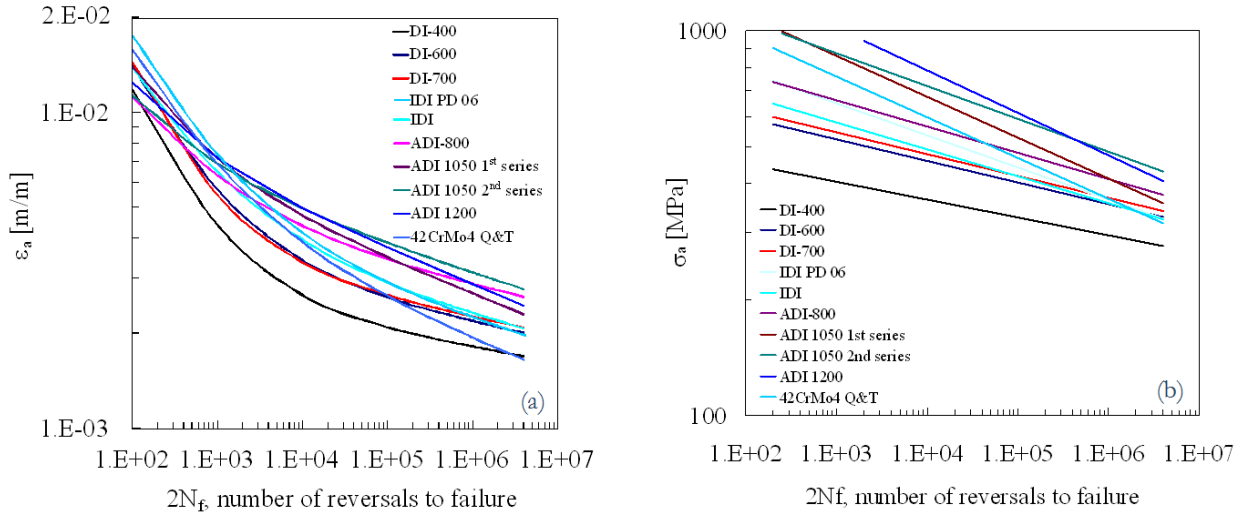

Figure 23: Manson-Coffin (a) and S-N curves (b) of all tested materials

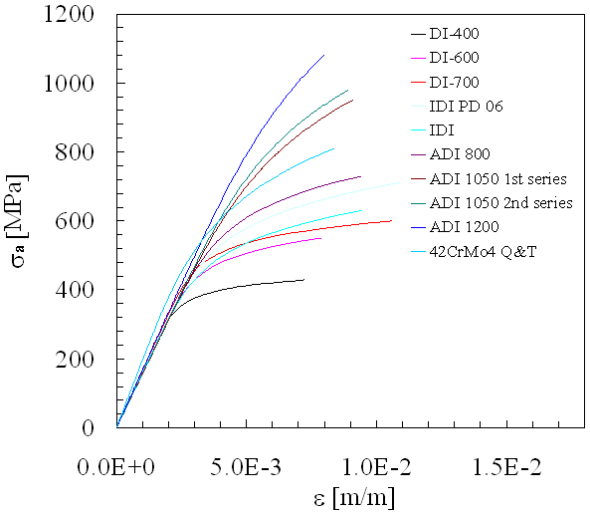

Figure 24: Cyclic stress-strain curves of all tested materials

CONCLUSIONS

In this paper the fatigue behaviour of ten different structural materials are analysed in terms of strain-life, stress life and cyclic stress-strain curves, which were evaluated according to standard procedures as well as following a recent approach proposed by the authors, that ensures the compatibility conditions are satisfied. As far as the materials investigated in the present paper are concerned, it was found that both procedures give very similar results in terms of strain-life curves, while for DI-700, ADI 800, both ADI 1050 series and ADI 1200 some differences were noticed in terms of cyclic stress-strain curves.

By considering the evolution of recorded stress amplitude during the fatigue tests, it was found that all tested materials does not attain stabilisation in a strict sense and then the hysteresis loops measured at 50% of fatigue life were considered for characterisation of cyclic properties.

The results of the present research confirm that a microstructure can be optimised for low-cycle or high-cycle fatigue behaviour. As an example, isothermal ductile irons showed high strain-controlled fatigue strength in the low-cycle fatigue, while austempered ductile irons with grade around 1000 demonstrated high fatigue strength in the high cycle regime. From a comparison of stress-strain cyclic curves with respect to the monotonic curve, it was seen that all cast irons present an hardening behaviour, while the tested structural steel is characterised by a softening behaviour.

REFERENCES

[1] E. Dowling, Mechanical Behavior of Materials, Pearson Prentice Hall (2007).
[2] ASTM E739-10$^{\varepsilon 1}$, Standard practice for statistical analysis of linear or linearized stress-life (S-N) and strain-life (ε-N) fatigue data (2010).
[3] A. Nieslony, C. Dsoky, H. Kaufmann, Int. J. Fatigue, 30 (2008) 1967.
[4] B. Atzori, G. Meneghetti, M. Ricotta, Key Engineering Materials, 488-489 (2012) 755.
[5] ASTM E606-98, Standard practice for strain-controlled fatigue testing (1998).
[6] C.R Williams, Y.-L. Lee, J.T. Rilly, Int J Fatigue, 25 (2003) 427.
[7] C. Boller, T. Seeger, Materials data for cycling loading, Elsevier (1987).